Journal of Power Sources 258 (2014) 272–280

Contents lists available at ScienceDirect

Journal of Power Sources

journal homepage: www.elsevier.com/locate/jpowsour

Swelling agent adopted decal transfer method for membrane electrode assembly fabrication

Doo Hee Cho, So Young Lee, Dong Won Shin, Doo Sung Hwang, Young Moo Lee*

Department of Energy Engineering, Hanyang University, Seoul 133-791, Republic of Korea

HIGHLIGHTS

- Swelling agent increases catalyst transfer ratio.
- Swelling agents change the catalyst layer structure and catalyst layer–membrane interface.
- Reduced overall resistance leads to significant improvement in single cell performance.

ARTICLE INFO

Article history:
Received 26 December 2013
Received in revised form
6 February 2014
Accepted 8 February 2014
Available online 18 February 2014

Keywords:
Decal transfer method
Swelling agent
Catalyst layer
Membrane electrode assembly
Proton exchange membrane fuel cell

ABSTRACT

The decal transfer method is regarded as an effective membrane electrode assembly (MEA) fabrication method for industrial processes due to the improved adhesion between the catalyst layers and the hydrocarbon membrane. In this study, three swelling agents (ethanol, 1,5-pentanediol and glycerol) are introduced to the conventional decal methods in order to improve both the transfer ratio of electrodes on the membrane surface and the electrochemical properties. These swelling agents affect the surface energy differences between the swollen catalyst layer and the membrane substrate. Swelling agents also change the structure of the catalyst layer during the preparation (hot pressing) of the MEA. Changing the catalyst layer structure by introducing swelling agents diminishes the charge transfer resistance and internal resistances of MEAs. These improved electrochemical properties lead to the remarkably enhanced single cell performance of a SPAES MEA of 1380 mA cm^{-2} at 0.6 V, compared to a SPAES MEA fabricated by the conventional decal method (500 mA cm^{-2}).

1. Introduction

Polymer electrolyte membrane fuel cells (PEMFCs) are regarded as a promising clean energy conversion device for potable and stationary applications due to low pollutant emission, high power density, relatively low operating temperature and proper stack system size [1]. However, the most substantial hurdle impeding commercialization of PEMFCs in energy conversion and power generation device markets is their lack of cost competitiveness. In PEMFC systems, about 50% of the PEMFC system price is the electrode, which consists of catalyst and binder [2].

Electrode research is a vigorous area in PEMFC systems, not only in terms of materials [3], but also in membrane electrode assembly (MEA) fabrication techniques such as sputter deposition, electro deposition and decal transfer processing. The decal transfer method for catalyst layer fabrication is more appropriate for industrial-scale production than the catalyst coated substrate (CCS) method [4,5]. Recent research on the decal transfer method has focused on the increased transfer ratio, which represents the proportion of loaded catalyst amount on membrane to that on substrate, and reduced electrochemical resistances to improve MEA durability. Cho et al. [6] introduced additives and a freezing step that increased long-term stability and improved the transfer ratio. Suzuki et al. [7] changed the composition of catalyst ink, which resulted in a change in the catalyst layer structures. Saha et al. [8] used a colloidal catalyst ink process in order to simplify the MEA fabrication. Moreover, studies have been conducted on liquid coating membranes, template supporting catalyst layers, modifying surface morphologies for water management, and so on [9–22].

Recently, sulfonated hydrocarbon polymer membranes have received attention as alternatives to perfluorosulfonic acid (PFSA) membranes. Hydrocarbon membranes have better fuel barrier properties, mechanical strength, thermal durability, wider operation conditions and a lower price than PFSA membranes [23,24].

* Corresponding author. Tel.: +82 2 2220 0525; fax: +82 2 2291 5982.
E-mail addresses: jms@hanyang.ac.kr, ymlee@hanyang.ac.kr (Y.M. Lee).

http://dx.doi.org/10.1016/j.jpowsour.2014.02.037
0378-7753/

Also, the fluorine-based chemistry can cause pollution to the atmosphere and the ecosystem [25]. Furthermore, PFSAs have a low glass transition temperature (T_g, 55 °C–130 °C), which decreases the mechanical properties of MEA [26], particularly at high temperature. For these reasons, hydrocarbon membranes are regarded as alternatives to PFSA membranes.

In general, aromatic hydrocarbon polymers have a higher T_g and better mechanical properties than PFSAs. In addition, the affinity between hydrocarbon membranes and perfluorinated polymer binders should be improved to prevent any delamination between the two layers. For these reasons, MEA fabrication with hydrocarbon membranes is conducted under high temperature (160–200 °C) and pressure (80–100 bar) conditions [13,15]. However, these harsh processing conditions can cause the degradation of membrane and catalyst layers, resulting in low final electrochemical MEA performance.

In this study, MEAs were fabricated based on two hydrocarbon membranes by a decal transfer method with three representative swelling agents, including ethanol, 1,5-pentanediol and glycerol, each having a different number of hydroxyl groups. It is our objective to study the catalyst layer transfer with surface thermodynamic analysis and to obtain improved electrochemical performance based on the two representative hydrocarbon membranes, poly(arylene ether sulfone) and sulfonated poly(phenylene sulfide sulfone nitrile), using three swelling agents.

2. Experimental

2.1. Materials

4,4′-Dichlorodiphenyl sulfone (DCDPS), 4,4′-dihydroxybiphenyl (BP), 2,6′-dichloro benzonitrile (DCBN), 4,4′-thiobisbenzenthiol (TBBT), potassium carbonate, toluene, 1-methyl-2-pyrrolidinone (NMP), dimethylacetamide (DMAc), glycerol, 1,5-pentanediol, and ethanol were purchased from Sigma Aldrich Co. (St. Louis, MO, USA). A 5 wt % Nafion® 2021 solution (EW = 1100, Dupont Co., Wilmington, DE, USA), 20 wt % carbon supported Pt catalyst (Pt/C, Alfa Aesar, Ward Hill, MA, USA) and tetrabutylammonium hydroxide (TBAOH 1.0 M solution in methanol, Aldrich, St. Louis, MO, USA) were used to prepare catalyst ink. DCDPS was sulfonated to 3,3′-disulfonated-4,4′-dichlorodiphenyl sulfone (SDCDPS, yield 90.8%) through direct sulfonation by using fuming sulfuric acid (30% free SO_3, Aldrich, St. Louis, MO, USA) [27]. Other reagents were used as received.

Sulfonated poly(arylene ether sulfone) (SPAES, degree of sulfonation = 40) copolymer was prepared following a procedure similar to that reported in the literature [27]. Sulfonated poly(-phenylene sulfide sulfone nitrile) (SPSSN, degree of sulfonation = 35) copolymer was synthesized following our previous study, as shown in Scheme 1 [28–30].

2.2. MEA fabrication

2.2.1. Membrane preparation

Na^+-form SPAES 40 and SPSSN 35 were dissolved in DMAc to a 15 wt % concentration. The polymer solutions were filtered with a 0.45-μm PTFE syringe filter and were degassed by sonication. Two kinds of polymer solutions were cast on glass plates, and were then dried under vacuum to remove solvent. The membranes were rinsed with deionized water and dried again under vacuum. The thickness of the resulting membranes was about 40 μm.

2.2.2. Decal transfer method

Catalyst slurry was prepared by mixing Pt/C, Nafion® solution, water, glycerol and tetrabutylammonium hydroxide (TBAOH). TBAOH was added to convert an acid-form catalyst slurry to a Na^+-form catalyst slurry. Catalyst slurry was stirred for 12 h and was sonicated for 30 min at room temperature to form a homogenous solution. Catalyst was loaded onto a polytetrafluoroethylene (PTFE) film using a brush with a 0.3 mg Pt cm^{-2} target catalyst weight.

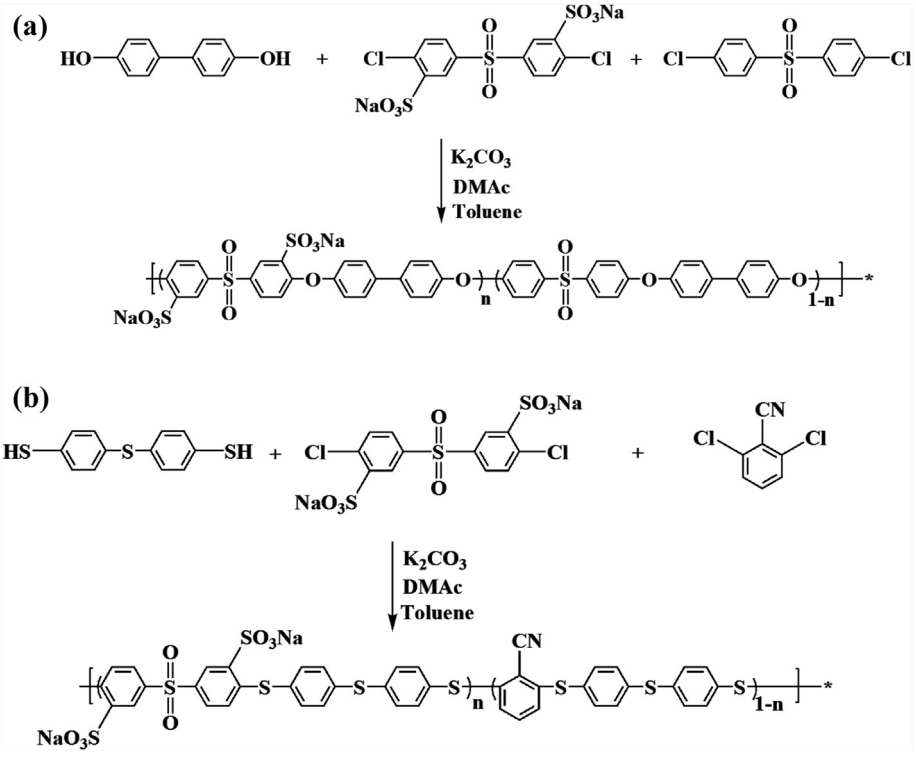

Scheme 1. Synthesis of (a) SPAES and (b) SPSSN.

Catalyst-loaded substrates were dried in a convection oven at 140 °C for 6 h.

Catalyst was transferred to the membrane by hot pressing for 5 min at 120 °C under 10 bar. Fabricated MEAs were soaked in 1 M sulfonic acid at 80 °C for 1 h, and were then rinsed several times with deionized water at 80 °C.

2.2.3. Swelling decal method

Three different swelling agents, ethanol, 1,5-pentandiol, and glycerol were brushed onto the catalyst layer; then, excessive swelling agent was wiped off. After swelling, the membrane was hot pressed with catalyst for 5 min at 120 °C under 10 bar to fabricate the MEA. Prepared MEAs were soaked in 1 M sulfuric acid at 80 °C for 1 h, and were then rinsed with deionized water at 80 °C [31,32].

2.3. Characterization

MEA performance was measured by assembling single cells with an active area of 5 cm^2. PTFE treated carbon paper (E-tek, NJ, USA) was used as a gas diffusion layer (GDL) for both the anode and cathode. Graphite collectors with aluminum end plates (CNL, Seoul, Korea) were used. The cell temperature was maintained at 80 °C. Hydrogen (130 cc min^{-1}) and oxygen (130 cc min^{-1}) at 100% relative humidity (RH) without any backpressure were used as the inflow gas at the anode and cathode, respectively. PEMFC performance was measured using a commercial test station (Won-A Tech, Korea).

Cross-sectional images of the catalyst layer in MEAs were obtained from a field emission high-resolution scanning electron microscope (FE-SEM, JSM-6330F, JEOL, Kyoto, Japan) to examine the thickness of the MEAs.

Contact angles of the catalyst layer and PTFE substrate were measured by a sessile drop contact angle method (PXH300, SEO, Suwon, Korea) with each swelling agent to calculate surface energy differences.

Electrochemical impedance spectroscopy (EIS) was performed using an EIS potentiostat (SI 1287, Solartron, Hampshire, UK). The impedance spectra were measured in constant-voltage mode at 0.6 V by sweeping frequencies over the range of 100 Hz–100 mHz with 10 points per decade. All EIS spectra were obtained under the same operating conditions as the polarization curve measurement test [33].

3. Results and discussion

3.1. Swelling decal method for hydrocarbon membrane and transfer ratio

Transfer states of various swelling agent decal methods on SPAES and SPSSN membranes are shown in Figs. 1 and 2, respectively. SPAES 40 and SPSSN 35 were named SPAES-X or SPSSN-X according to the kind of adopted swelling agents used, where X is N without a swelling agent N, E is with ethanol, P is with 1,5-pentanediol, and G is with glycerol; N was set as a reference.

The catalyst transfer ratio was calculated by using the following equation

$$T = \frac{w_a - w_b}{w_a - w_c} \times 100(\%) \quad (1)$$

where w_a, w_b and w_c represent substrate weight with catalyst layer, substrate weight with residual catalyst layer after transfer and substrate weight, respectively. The results are listed in Table 1.

Regardless of membrane materials, the catalyst transfer ratio T was determined by the type of swelling agents, as shown in Fig. 1 and Table 1. Figs. 1(b) and 2(b) represent the uneven transfer states of the catalyst layers for SPAES-E and SPSSN-E. These membranes had the lowest catalyst transfer ratio of about 85%. In contrast, the MEA fabricated with glycerol as a swelling agent (SPAES-G and SPSSN-G) achieved the highest transfer ratio of over 99%.

This phenomenon can be caused by the catalyst swelling step. Decal transfer is based on the differences in surface energy when various swelling agents are applied to the catalyst layer and PTFE substrate (see Table 2). The surface energy can be obtained from Young's equation (Eq. (2)). Here, surface energy differences between the swelling agent with catalyst layer and PTFE substrate

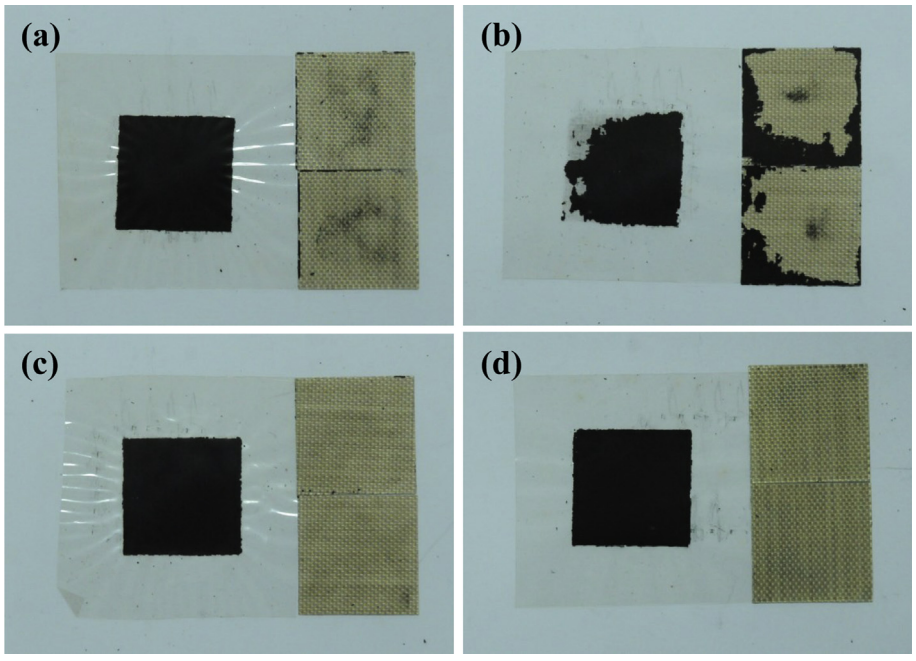

Fig. 1. Fabricated SPAES 40 MEAs: (a) without swelling agent, (b) ethanol, (c) 1,5-pentandiol and (d) glycerol.

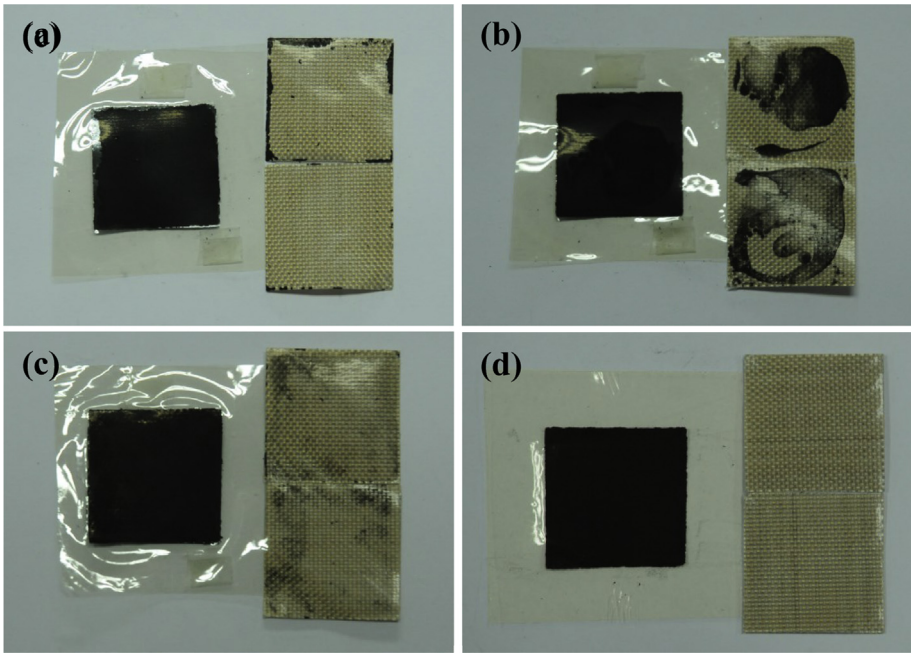

Fig. 2. Fabricated SPSSN 35 MEAs: (a) without swelling agent, (b) ethanol, (c) 1,5-pentandiol, and (d) glycerol.

were calculated with a modified Young's equation (Eq. (3)) with measured contact angles and the surface tension of each swelling agent, as shown in Fig. 3 and Table 2.

$$\gamma_{sg} - \gamma_{sl} - \gamma_{lg}\cos\theta = 0 \tag{2}$$

$$\begin{aligned}\Delta\gamma &= \gamma_{CS} - \gamma_{PS} = \left(\gamma_{gC} - \gamma_{gS}\cos\theta_C\right) - \left(\gamma_{gP} - \gamma_{gS}\cos\theta_P\right) \\ &= \left(\gamma_{gS,on\ P}\cos\theta_P - \gamma_{gS,on\ C}\cos\theta_C\right) + \left(\gamma_{gC} - \gamma_{gP}\right)\end{aligned} \tag{3}$$

Here, γ is the surface energy and subscripts s, g, l, S, P and C represent the solid, gas, liquid, swelling agent, PTFE substrate and catalyst layer, respectively. For example, subscripts gC and PS indicate the interface between the gas with catalyst layer and interface between PTFE substrate with swelling agents, respectively. The pristine sample without any swelling agent was defined as a constant B, as described in Eq. (4). The values of swelling agent adopted samples are calculated by Eq. (5), and are represented with a value B.

$$\Delta\gamma_{Non} = \left(\gamma_{gC} - \gamma_{gP}\right) = B \tag{4}$$

Therefore, Eq. (3) can be rewritten as,

$$\Delta\gamma = \left(\gamma_{gS,on\ P}\cos\theta_P - \gamma_{gS,on\ C}\cos\theta_C\right) + B \tag{5}$$

Calculated surface energy differences represent the direction of migration of swelling agent during hot pressing. Migration of swelling agent into the catalyst–substrate interface or the center of the catalyst layer affected catalyst transfer ratio values, as denoted in Table 2. Accordingly, catalyst transfer ratio values corresponded to the order of surface energy differences. Note that glycerol swelled the catalyst layer and migrated to the more attractive domain side of the PTFE substrate. This migration phenomenon was obviously induced by a surface energy difference between glycerol and the PTFE substrate. The calculated surface energy difference ($\Delta\gamma$) of the glycerol swollen sample is $53.36 + B$ mN m^{-1}. In this case, the migrated glycerol helped demount the catalyst layer from PTFE with the highest catalyst layer transfer ratio of 99%. On the other hand, in the case of the ethanol swollen sample, $\Delta\gamma = -9.30 + B$ mN m^{-1}, indicating that the ethanol remained in the catalyst layer. The remaining ethanol made the catalyst layer easy to split into the transferred part and residual part, as shown in Figs. 1(b) and 2(b).

3.2. Catalyst layer structure and electrochemical properties

Swelling agent adopted samples have different ohmic resistances, charge transfer resistance and double layer capacitance [33–35]. The ohmic resistance consisted of an internal resistance and an interfacial resistance of the gas diffusion layer (GDL), catalyst layer and membrane itself, as shown in Scheme 2. Here, we assume that the sum of the internal resistance of SPAES 40 with a GDL is set as a constant resistance (R_1), and SPSSN 35 with a GDL is modeled as another constant resistance (R_2). The difference in interfacial resistance between the catalyst layer and GDL or membrane is caused by the effect of each swelling agent. Attachment of each interface is a dominant factor influencing interfacial resistances of MEA. SPAES-P and SPSSN-G had lower interfacial resistance values ($53 - R_1$, $52 - R_2$ mohm cm^{-2}) than

Table 1
Fabricated MEAs catalyst layer transfer ratio.

	Swelling agent			
	Non	Ethanol	1,5-Pentandiol	Glycerol
SPAES 40	93.2%	85.3%	98.1%	99.8%
SPSSN 35	91.2%	82.1%	97.6%	99.7%

Table 2
Contact angles and surface tension differences.

	Swelling agent			
	Non	Ethanol	1,5-Pentandiol	Glycerol
Contact angle on catalyst layer	–	10.1°	134.4°	153.7°
Contact angle on PTFE substrate	–	55.7°	87.2°	93.6°
Surface tension (mN m^{-1})		22.10	43.30	64.00
Surface energy difference (mN m^{-1})	B	$-9.30 + B$	$32.41 + B$	$53.36 + B$

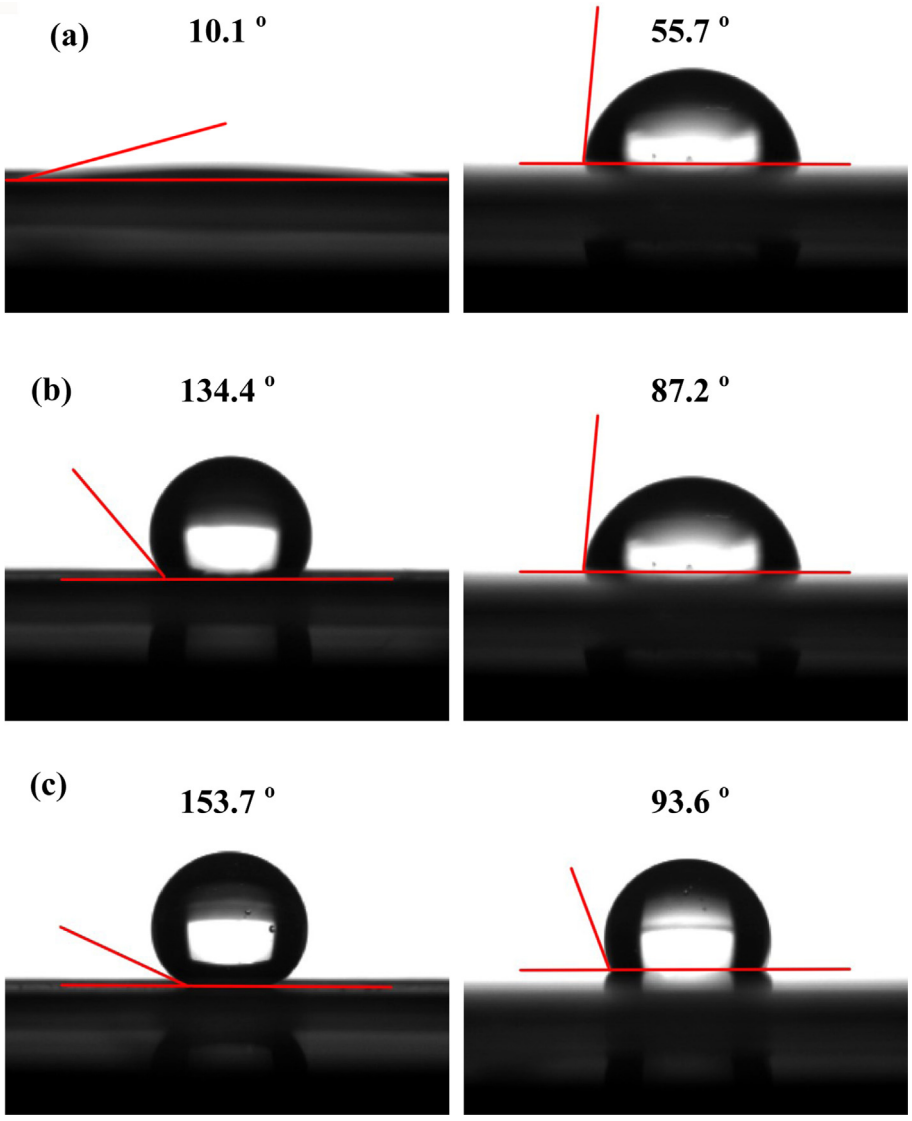

Fig. 3. Contact angles of the catalyst layer (left side), and substrate (right side) with (a) ethanol, (b) 1,5-pentandiol and (c) glycerol.

SPAES-N; further, SPSSN-N had the highest interfacial resistance values ($175 - R_1$, $125 - R_2$ mohm cm^{-2}). As a result, attachments at both interfaces are influenced by swelling agents. Moreover, the appropriate swelling agent for each membrane was different and varied with the chemical structure of the membrane.

Charge transfer resistance is affected by the structure of the catalyst layer, which changed with swelling agent activity during transfer to the membrane. In order to examine this phenomenon, overall porosities of the catalyst layer were measured to observe the change of catalyst layer structure. The overall porosities of the catalyst layer were calculated by Eqs. (6) and (7) with catalyst layer thickness and actual loadings of Pt/C and Nafion® ionomer. The thickness of the catalyst layer was determined from the cross-sectional SEM images of MEA, as shown in Fig. 4.

$$t_{\text{compact}} = \frac{m_C}{\rho_C} + \frac{m_{Pt}}{\rho_{Pt}} + \frac{m_{\text{Nafion}}}{\rho_{\text{Nafion}}} \tag{6}$$

$$\varepsilon = \frac{(t_{CL} \times A) - t_{\text{compact}}}{(t_{CL} \times T)} \tag{7}$$

Here, t_{compact}, t_{CL}, m, ρ, C and ε represent compact thickness, measured catalyst layer thickness, weight, density, carbon and overall porosity, respectively. Densities (ρ) of carbon, platinum and

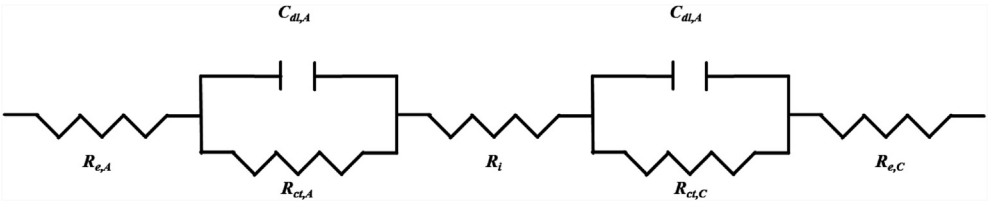

Scheme 2. Schematic circuit of MEA.

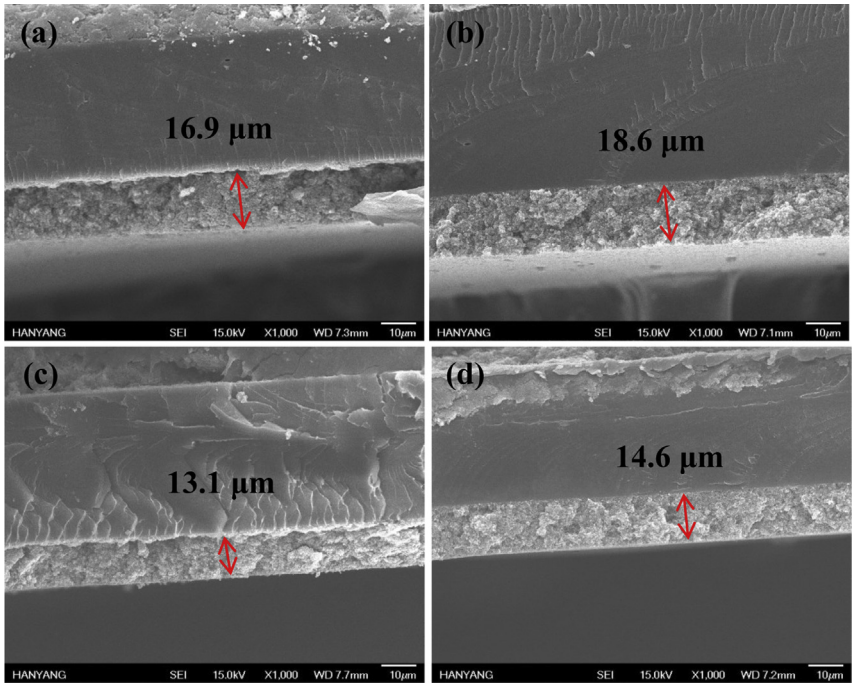

Fig. 4. SEM cross-section images of (a) SPAES-N, (b) SPAES-E, (c) SPAES-P and (d) SPAES-G.

Nafion® were assumed to be 2.0, 1.8 and 21.45 g cm^{-3}, respectively [7]. Calculated compact thickness, $t_{compact}$, was 7.90 μm, with the assumption of a densely packed state without pores. The overall porosity, ε, was calculated from t_{CL}, T and $t_{compact}$ and is listed in Table 3.

Charge transfer resistance values of SPAES 40 and SPSSN 35 depend on swelling agents. The charge transfer resistances were measured by EIS analysis. Table 3 and Fig. 5 show the comparison of overall calculated porosities to measure charge transfer resistances [36,37]. SPAES-P (68 m ohm cm^{-2}) and SPSSN-P (57 m ohm cm^{-2}) had the lowest charge transfer values with the lowest ε value (40.5%) of the catalyst layer, whereas SPAES-E (108 m ohm cm^{-2}) and SPSSN-E (93 m ohm cm^{-2}) had the highest charge transfer resistance values with the highest ε value (67.4%). This phenomenon indicates that each swelling agent changes the catalyst layer structure in a manner related to the charge transfer resistance.

Based on these results, the ohmic resistance of MEA depends on a combination of interfacial adhesion and catalyst layer structure. For example, SPSSN-P showed lower charge transfer resistance (57 m ohm cm^{-2}) than SPSSN-G (67 m ohm cm^{-2}), while the interfacial resistance value of SPSSN-P (98 − R_2 m ohm cm^{-2}) was higher than that of SPSSN-G (52 − R_2 m ohm cm^{-2}). Therefore, SPSSN-G exhibited a lower overall resistance value (119 m ohm cm^{-2}) than SPSSN-P (153 m ohm cm^{-2}), unlike SPAES-P.

3.3. Single cell performance

The prepared MEAs were tested for PEMFC single cell performance by feeding fully humidified H_2/O_2 at 80 °C, as shown in Fig. 6. Single cell performance is determined by several electrochemical factors. The open circuit voltage (OCV) is the electrochemical potential of the water formation reaction from hydrogen and oxygen. Three major factors, activation loss, ohmic loss and concentration loss, drop the voltage from the OCV.

Table 3
Overall porosity varies with swelling agents.

	Swelling agent			
	Non	Ethanol	1,5-Pentandiol	Glycerol
Catalyst layer thickness (μm)	16.9	18.6	13.1	14.6
Overall porosity ε (%)	57.1	67.4	40.5	46.0

The OCV depends on reaction temperature, and the theoretical voltage was calculated by Eq. (8):

$$E = \frac{-\Delta\bar{g}_f}{2F} \tag{8}$$

where E is the OCV and $\Delta\bar{g}_f$ is the Gibbs free energy difference of chemical reactions in the PEMFC. At 80 °C, $\Delta\bar{g}_f$ is −228.2 kJ $mole^{-1}$, and the calculated OCV is 1.18 V [1]. However, the actual OCV was lower than the theoretical value, about 0.96 V–0.98 V, due to fuel crossover and internal current loss.

At low current density area, activation loss is the prevailing reason for rapid voltage loss in the PEMFC. This activation loss relates to the electrochemical reaction speed, including splitting hydrogen into protons, passing protons through electrolyte, and combining protons, electrons and oxygen in water. This can be determined by the Tafel equation:

$$\eta_{act} = A\ln\left(\frac{i}{i_0}\right) \tag{9}$$

Here, η_{act} represents activation loss and A is the reaction speed constant (0.03043 V at 80 °C), which is related to catalyst material and reaction temperature. As shown in Figs. 6–8, single cell performance was lower when η_{act} was higher at low current density area. Thus, SPAES-N and SPSSN-E showed the lowest performance in each sample group for low current density area.

The ohmic loss, η_{ohm}, is the main factor in the mid current density region. This ohmic loss is mainly determined by the electrochemical properties of MEA [34]. The ohmic resistance of MEA mainly consisted of membrane resistance, catalyst layer impedance and interfacial resistance between the membrane and catalyst layer. This can be simply expressed by Ohm's law [1]:

$$\eta_{ohm} = ir \tag{10}$$

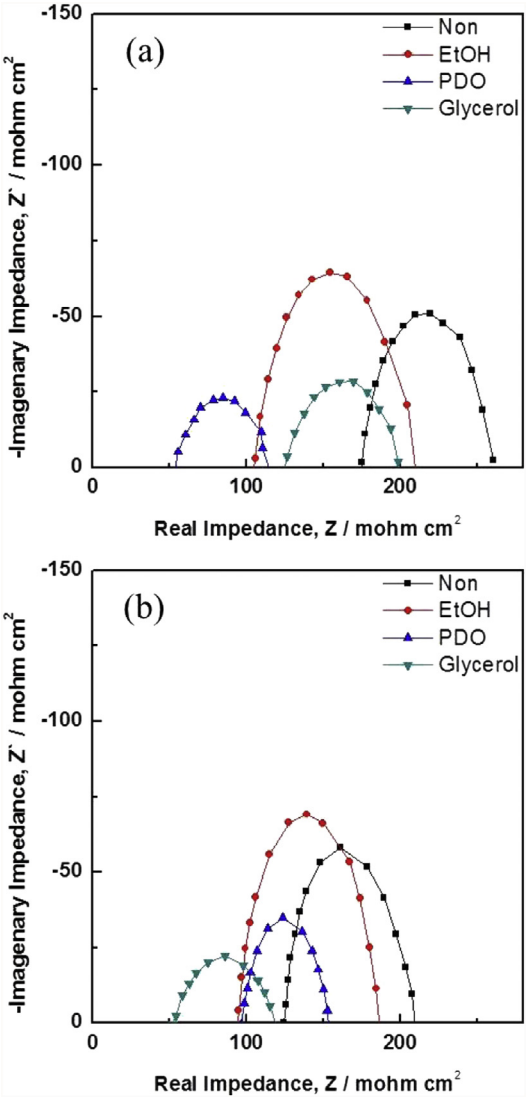

Fig. 5. EIS measurement at 0.6 V for (a) SPAES 40 and (b) SPSSN 35.

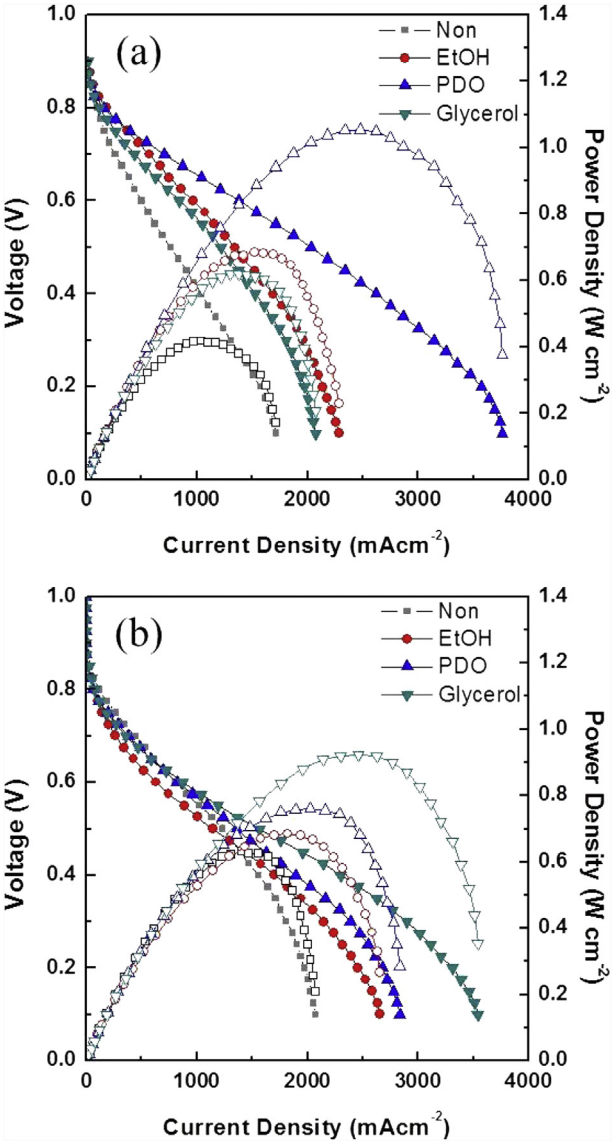

Fig. 6. Single cell performance of fabricated MEAs with swelling agents for (a) SPAES 40 membrane and (b) SPSSN 35 membrane.

When comparing SPSSN-E and SPSSN-N, SPSSN-N had a lower η_{act} and higher ohmic resistance than SPSSN-E. So, SPSSN-N exhibited higher performance than SPSSN-E at low current density area, whereas the performance of SPSSN-N was lower than that of SPSSN-E in the mid current density area. Also, comparing SPAES-E with SPAES-G, both samples had similar ohmic resistance values (208 m ohm cm^{-2} and 200 m ohm cm^{-2}, respectively). Furthermore, the voltage drop aspect was the same due to the similarity in resistance, while SPSSN-G showed improved performance due to the differences in η_{act}.

The concentration loss, η_{con}, is related to the dramatic potential drop at high current density area. This phenomenon occurs due to a fuel transport problem, which is caused by reaction rate, fuel supplements and water management. The concentration loss was calculated by Eq. (11):

$$\eta_{con} = \frac{RT}{2F}\ln\left(1 - \frac{i}{i_l}\right) \tag{11}$$

Actual single cell performance was calculated from Eq. (12) [1,38,39].

$$V = E - \eta_{act} - \eta_{ohm} - \eta_{con} \tag{12}$$

The single cell performance of the SPAES 40 membrane is described in Fig. 6(a) and was decomposed into three factors of voltage loss in Fig. 7. SPAES-N showed a sharp increase in ohmic loss due to the high interfacial resistance and charge transfer resistance. In contrast to SPAES-N, SPAES-P exhibited the lowest increase in ohmic loss due mainly to better adhesion between the membrane and catalyst layer and to a proper catalyst layer structure.

The effect of swelling agents on SPSSN 35 membrane single cell performance was depicted in Figs. 6(b) and 8. In general, the single cell performances of MEA are determined by ohmic resistance. Note that SPSSN-E and SPSSN-N performed poorly at low current density area (442 mA cm^{-2} and 264 mA cm^{-2} each at 0.7 V), which was caused by an uneven catalyst layer transfer state and increased activation loss. However, SPSSN-E overtakes the performance of SPSSN-N due to its lower ohmic resistance. Unlike the SPAES 40 membrane system, SPSSN-G showed the highest performance (2302 mA cm^{-2} at 0.4 V), induced by better compatibility between glycerol and the SPSSN 35 membrane as elucidated with EIS measurements.

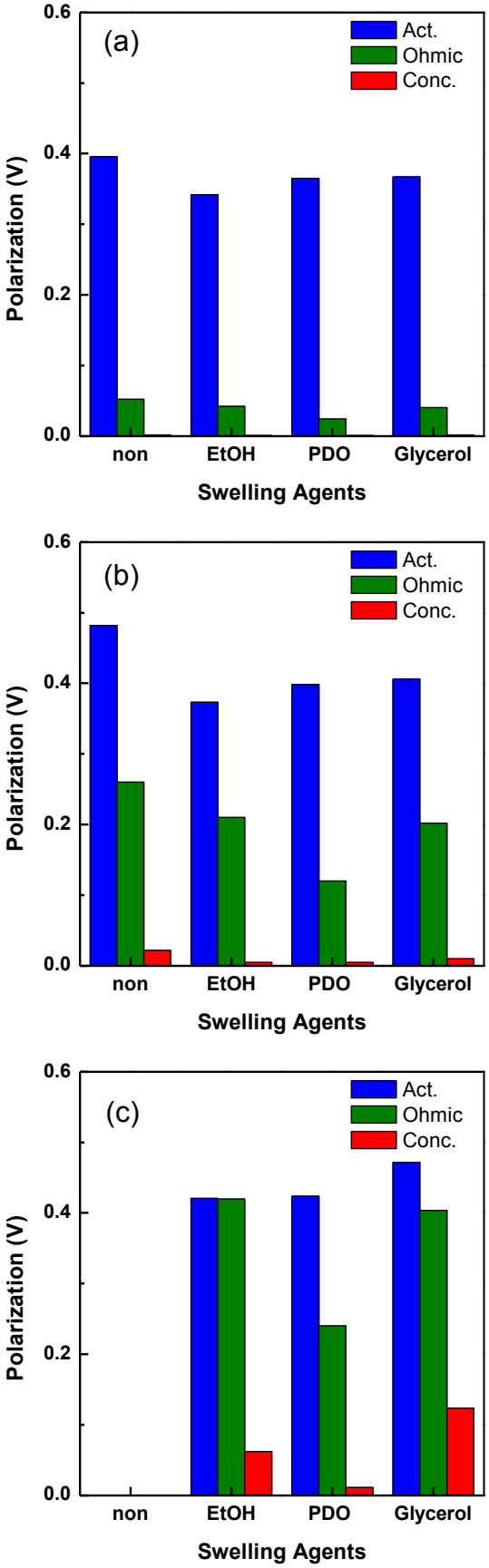

Fig. 7. Electrochemical analysis of an SPAES 40 membrane with each swelling agent at (a) 200 mA cm^{-2}, (b) 1000 mA cm^{-2} and (c) 2000 mA cm^{-2}.

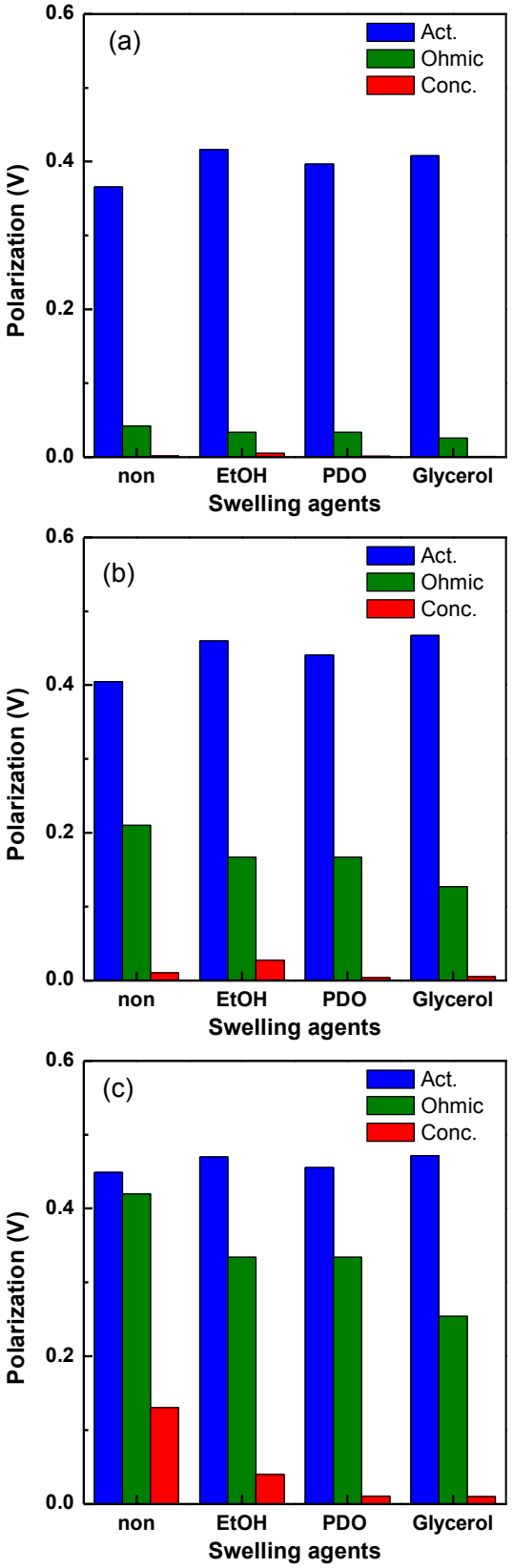

Fig. 8. Electrochemical analysis of an SPSSN 35 membrane with each swelling agent at (a) 200 mA cm^{-2}, (b) 1000 mA cm^{-2} and (c) 2000 mA cm^{-2}.

4. Conclusions

In the swelling decal method, the catalyst layer transfer ratio increased with large surface energy differences between a swelling agent with a catalyst layer and the PTFE substrate. Because of the large surface energy differences, the swelling agent migrated to the PTFE substrate or to the middle of the catalyst layer. The electrochemical properties, such as double layer capacitance, interfacial resistance and ohmic resistance, were changed due to catalyst layer modification from swelling agents. Ohmic resistance of catalyst layers showed the lowest value when 1,5-pentanediol was used as a swelling agent for two representative polymer membranes (SPAES and SPSSN). In contrast, ethanol adopted membranes and MEAs thereof showed the highest ohmic resistance in a catalyst layer. Interestingly, the interfacial resistance between the membrane and catalyst layer showed different trends even for the same swelling agent with two different membranes. For the SPSSN membrane, SPSSN-G ($52 - R_2$ m ohm cm^{-2}) showed a lower interfacial resistance than SPSSN-P ($98 - R_2$ m ohm cm^{-2}). On the other hand, the SPAES membrane showed better affinity with 1,5-pentanediol ($53 - R_1$ m ohm cm^{-2}) than glycerol ($124 - R_1$ m ohm cm^{-2}). In summary, swelling agents played an important role in reducing the interfacial resistance between the membrane and catalyst layer, resulting in an enhanced adhesion and transfer rate, and, thus, high PEMFC single cell performance of the MEA. For further MEA fabrication, appropriate swelling agents need to be investigated with minimal interfacial resistance between the membrane and catalyst layer.

Acknowledgments

This work was supported by the Nano·Material Technology Development through the National Research Foundation of Korea (NRF) funded by the Ministry of Education, Science and Technology (2012M3A7B4049745).

References

[1] C. Rayment, S. Sherwin. Introduction to Fuel Cell Technology, University of Notre Dame, May 2, 2003.
[2] S. Sharma, B.G. Pollet, J. Power Sources 208 (2012) 96–119.
[3] B. Millington, S. Du, B.G. Pollet, J. Power Sources 196 (2011) 9013–9017.
[4] J.-H. Wee, K.-Y. Lee, S.H. Kim, J. Power Sources 165 (2007) 667–677.
[5] S. Thanasilp, M. Hunsom, Fuel 89 (2010) 3847–3852.
[6] H.J. Cho, H. Jang, S. Lim, E. Cho, T.-H. Lim, I.-H. Oh, H.-J. Kim, J.H. Jang, Int. J. Hydrogen Energy 36 (2011) 12465–12473.
[7] T. Suzuki, S. Tsushima, S. Hirai, Int. J. Hydrogen Energy 36 (2011) 12361–12369.
[8] M.S. Saha, D.K. Paul, B.A. Peppley, K. Karan, Electrochem. Commun. 12 (2010) 410–413.
[9] Y.J. Yoon, T.-H. Kim, S.U. Kim, D.M. Yu, Y.T. Hong, J. Power Sources 196 (2011) 9800–9809.
[10] B. Liu, S. Creager, Electrochim. Acta 55 (2010) 2721–2726.
[11] W. Song, H. Yu, L. Hao, Z. Miao, B. Yi, Z. Shao, Solid State Ionics 181 (2010) 453–458.
[12] N. Rajalakshmi, K.S. Dhathathreyan, Chem. Eng. J. 129 (2007) 31–40.
[13] S.Q. Song, Z.X. Liang, W.J. Zhou, G.Q. Sun, Q. Xin, V. Stergiopoulos, P. Tsiakaras, J. Power Sources 145 (2005) 495–501.
[14] S. Jeon, J. Lee, G.M. Rios, H.-J. Kim, S.-Y. Lee, E. Cho, T.-H. Lim, J. Hyun Jang, Int. J. Hydrogen Energy 35 (2010) 9678–9686.
[15] J.H. Cho, J.M. Kim, J. Prabhuram, S.Y. Hwang, D.J. Ahn, H.Y. Ha, S.-K. Kim, J. Power Sources 187 (2009) 378–386.
[16] T.J. Mason, J. Millichamp, T.P. Neville, P.R. Shearing, S. Simons, D.J.L. Brett, J. Power Sources 242 (2013) 70–77.
[17] W.-K. Kim, K.A. Sung, K.-H. Oh, M.-J. Choo, K.Y. Cho, K.-Y. Cho, J.-K. Park, Electrochem. Commun. 11 (2009) 1714–1716.
[18] G. Liu, M. Wang, Y. Wang, F. Ye, T. Wang, Z. Tian, X. Wang, Int. J. Hydrogen Energy 37 (2012) 8659–8663.
[19] C.-Y. Jung, W.-J. Kim, S.-C. Yi, Int. J. Hydrogen Energy 37 (2012) 18446–18454.
[20] G. Bender, T.A. Zawodzinski, A.P. Saab, J. Power Sources 124 (2003) 114–117.
[21] A.B. Deshmukh, V.S. Kale, V.M. Dhavale, K. Sreekumar, K. Vijayamohanan, M.V. Shelke, Electrochem. Commun. 12 (2010) 1638–1641.
[22] T.T. Ngo, T.L. Yu, H.-L. Lin, J. Power Sources 225 (2013) 293–303.
[23] C.H. Park, C.H. Lee, M.D. Guiver, Y.M. Lee, Prog. Polym. Sci. 36 (2011) 1443–1498.
[24] A. Roy, M.A. Hickner, O. Lane, J.E. McGrath, J. Power Sources 191 (2009) 550–554.
[25] P.R. Resnick, J. Fluor. Chem. 128 (2007) 570.
[26] T. Xie, Nature 464 (2010) 267–270.
[27] F. Wang, M. Hickner, Y.S. Kim, T.A. Zawodzinski, J.E. McGrath, J. Membr. Sci. 197 (2002) 231–242.
[28] D.W. Shin, S.Y. Lee, N.R. Kang, K.H. Lee, M.D. Guiver, Y.M. Lee, Macromolecules 46 (2013) 3452–3460.
[29] S.Y. Lee, N.R. Kang, D.W. Shin, C.H. Lee, K.-S. Lee, M.D. Guiver, N. Li, Y.M. Lee, Energy Environ. Sci. 5 (2012) 9795.
[30] D.S. Phu, C.H. Lee, C.H. Park, S.Y. Lee, Y.M. Lee, Macromol. Rapid Commun. 30 (2009) 64–68.
[31] Y.S. Kim, K.-S. Lee, T.Q.T. Rockward, in, Los Alamos National Security, LLC, USA. 2010, pp. 14.
[32] Y.S. Kim, K.-S. Lee, T.Q.T. Rockward, in, Los Alamos National Security, LLC, USA, 2010, pp. 13, Chemical Indexing Equivalent to 153:408238 (WO).
[33] T.J.P. Freire, E.R. Gonzalez, J. Electroanal. Chem. 503 (2001) 57–68.
[34] P.M. Gomadam, J.W. Weidner, Int. J. Energy Res. 29 (2005) 1133–1151.
[35] W.-J. Ahn, S.-D. Yim, Y.-W. Choi, Y.-J. Sohn, S.-H. Park, Y.-G. Yoon, G.-G. Park, T.-H. Yang, K.-B. Kim, Electrochim. Acta 56 (2011) 7732–7739.
[36] S. Leinad Gnana Lissy, S. Pitchumani, K. Jayakumar, Mater. Chem. Phys. 76 (2002) 143–150.
[37] S. Yuan, C. del Rio, M. López-González, X. Guo, J. Fang, E. Riande, J. Phys. Chem. C 114 (2010) 22773–22782.
[38] M.V. Williams, H.R. Kunz, J.M. Fenton, J. Electrochem. Soc. 152 (2005) A635.
[39] C.-Y. Jung, W.-J. Kim, S.-C. Yi, Int. J. Hydrogen Energy 37 (2012) 7654–7668.